Journal of Operation and Automation in Power Engineering

Vol. 11, No. 4, Dec. 2023, Pages: 258-267

http://joape.uma.ac.ir

Torque Ripple Reduction of the Position Sensor-less Switched Reluctance Motors Applied in the Electrical Vehicles

A. Dejamkhooy, A. Ahmadpour*

Department of Electrical Engineering, University of Mohaghegh Ardabili, Ardabil, Iran

Abstract— *The Switched Reluctance Motors (SRMs) not only are low cost for industry applications, but also they could work in various conditions with high reliability and efficiency. However, usage of these motors in high speeds applications under discrete mode causes decreasing the efficiency. In this paper, a new optimized control method based on the various Torque Sharing Functions (TSFs) and optimization algorithms is proposed for Minimum Torque Ripple Point Tracking (MTRPT) of a 4-phase SRM with 6/8 poles. In this method, turn-on and commutation angles are controlled based on the lookup table. The proposed method could adjust the rapid variations of the current in the starting mode of SRM. To show the robustness of the proposed approach, a real case study is considered, the control method is applied in an Electric Vehicle (EV) mechanism, and its performance is assessed in various motion states such as acceleration, breakage, and steady-state. Also, the position sensor for the studied EV is neglected, which could reduce the extra costs. There are two various scenarios considered for solving the problem. First, the turn-off and turn-on angles are controlled, and the commutation angle is fixed. The results show the robustness of the proposed method with about 90 % diminishing the torque ripple, compared to when all mentioned angles are fixed. In the second step, based on a lookup table, instead of using complex analytical methods, the turn-on angle is controlled. Therefore, a variable turn-on angle proportional to the applied speed is applied to the commutation control system of SRM. Besides, a lookup table is created to restrain the reduction of the turn-off angle. The simulation results are compared to other previous methods, and the worth of the proposed method is shown.*

Keywords—Switched Reluctance Motors, Minimum Torque Ripple Point Tracking, Torque Sharing Functions, Electric Vehicles.

1. INTRODUCTION

1.1. Motivation

The usage of Electrical Vehicles (EVs) has various benefits, which finally, efficiently decrease the emissions of greenhouse gases. Therefore, interest in various traction systems is enhanced for EVs and Hybrid EVs (HEVs). In recent years, several electrical motors have been introduced, such as induction motors, brushless DC motors, and Switched Reluctance Motors (SRMs) [1, 2]. The SRMs, due to their simpler structures, lower cost, and higher resilience under various conditions, are primarily used in EVs [3]. An SRM includes poles for rotor and stator, separately. Also, SRMs have no Permanent Magnet (PM), and windings are employed in the stator. This causes motor works with high speeds as well as high-temperature conditions. The variations of reluctance help to produce torque in SRMs. Owing to salient poles on both sides of the motor, the electrified winding attracts the nearest rotor pole and the phase inductance variates. It should be noted that the rotational motion of SRM is enabled due to a control drive of its phase by a power converter.

However, the special structure of SRM, i.e. doubly salient, and its excitation produced by a single source, lead to non-linear output characteristics. Therefore, due to this drawback, the ripple of torque and acoustic noise are obtained with high values. Braking and accelerating in cars is a continuous mechanical movement. When a car is accelerating and needs extra power, it needs continuous torque without fluctuating. Also, when an obstacle is reached, the force should be reduced. So, a quick reaction is necessary to reduce the torque. In the cases of conventional controllers, the fluctuations of the accelerator and brake pedals have caused user dissatisfaction. Therefore, it needs an optimal control to mitigate the mentioned fluctuations.

1.2. Literature Review

The Torque Sharing Function (TSF) for current profiling is the most common method among the Minimum Torque Ripple Point Tracking (MTRPT) techniques [4–6]. The TSF also includes various types as linear, cubic, exponential, and so on, which are studied in plenty of papers. In [7], a novel nonlinear type of TSF is proposed to increase the efficiency and obtain MTRPT. The authors of [4] proposed both online and offline TSF that work with a variation of operation point and flux linkage, respectively. In the same way as [4], a novel offline TSF is applied to SRM that could be controlled by the profile of flux linkage [8]. A new TSF for SRM in [9] is proposed to reach a forecastable control. A novel forecastable multi-objective optimization model is proposed in [10] that encourages the TSF control.

The mentioned studies don't consider the turn-off/on angles in their proposed methods. The control of SRMs, due to their nonlinear features, is a challenge. To cope with this problem, the model of SRMs is often linearized, and the controller is designed. In [11], the Dahlin controller family is proposed for adaptive control in SRM. A comprehensive comparison of various linearized models is carried out in [12]. Besides, the authors proposed a new fixed PI controller that is based on SRM parameters. The authors of [13] presented a new small-signal model of optimal control of speed and current in SRM drive. In [14], the PI controller is composed of TSF that could control the hysteresis current.

The analytic modeling is one of the main challenges to reaching

Received: 30 Nov. 2021
Revised: 24 Jun. 2021
Accepted: 11 Sep. 2022
*Corresponding author:
E-mail: majiddejam@gmail.com (A. Dejamkhooy)
DOI: 10.22098/JOAPE.2023.9908.1694
Research Paper

a robust control system of SRMs. In order to cope with this issue, this paper presents a novel method that could consider the TSF at the same time that the SRM controller is designed, and it minimizes the back-EMF effects. In the next step, a robust, fast, and low-cost controller is needed for SRM control. In [15], a predictive current controller is proposed for the coupled SRM based on the net flux method. The results of [15] show the enhancement of the torque regulation. An analysis of dynamic current control methods for SRM drives is done in [16]. In this study, the authors concluded that the PI controllers have better results than others due to lower sensitivity to the errors of models. A current deadbeat controller with active thermal management is used in [17] for optimal MTRPT of SRM. However, the applied method couldn't be a worthwhile technique for Direct Torque Control (DTC) in SRMs due to obtaining the reference value in a single cycle causes the high effort of the control process. A fact in [18] is validated by experimental results that various methods could be effective in some cases and act weakly in others. In this recent study, the authors presented the performance and sensitivity of discrete-time PI controller, deadbeat control, and Dahlin controller in both dynamic and steady-state mode for PM–Synchronous Motor (PMSM). In [19], a novel design of SRM is proposed with the aim of MTRPT. Also, the optimization results are evaluated with experimental outputs of a prototype of the proposed structure. The application of SRM in EV is studied in [20], and a new control strategy is proposed to minimize the torque ripple based on TSFs. A new TSF is presented in [21] for torque ripple reduction of SRMs, which could establish the new current reference generation strategy. The propulsion applications with SRMs are the issue of [22] that effort to reduce their torque ripple and acoustic noise in EVs and electric bikes. In a recent work [23], the authors tried to propose an indirect torque control strategy for SRMs by introducing a novel TSF.
In [24], a novel control based on field-oriented control without sensor is proposed to detect the current fault of an induction motor. Moreovere, authors of [25] used the presented method in [24], and combined it with Direct Torque Control (DTC) to control a three phase induction motor. In [26], a vector control method is applied on the three phase induction motor under faults conditions. In [27], the Direct Instantaneous Torque Control (DITC) is poroposed for generating/braking mode of SRM. The results show the higher efficiency and lower torque ripple in comparison with DTC. In [28], a sliding mode DITC cruise control is applied in the SRM drive with aim of MTRPT and speed tracking. In [29], a novel hybrid control method based on Model Predictive Control (MPC) and TSF has been presrnted to decrease the torque ripple of SRM. The Maximum Torque per Ampere (MTPA) control strategy as a novel method is studied in [30] and applied on a three phase SRM to decrease the torque ripple.

1.3. Paper Contributions

In this paper, the authors proposed the following contributions:

- Preparing a novel control strategy of SRM based on TSFs to reduce the torque ripple.
- The turn-on angle and commutation angle are controlled based on the lookup table.
- The control method is applied in an EV mechanism, and its performance is studied.
- Also, the proposed method could adjust the rapid variations of the current in the starting mode of SRM.

1.4. Paper Organization

The paper organization is as follows. In Section 2, the dynamic model of SRM is studied. In Section 3, the proposed method is presented. Section 4 presents the results of the simulation, and a discussion of the results is debated. Finally, the conclusion is presented in Section 5.

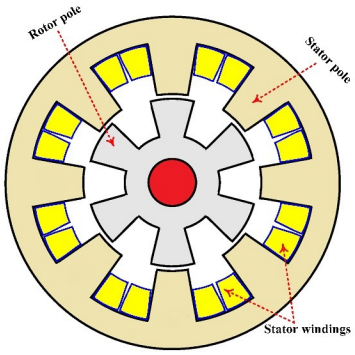

Fig. 1. The structure of the studied 4-phase SRM with 8 stator poles and 6 rotor poles

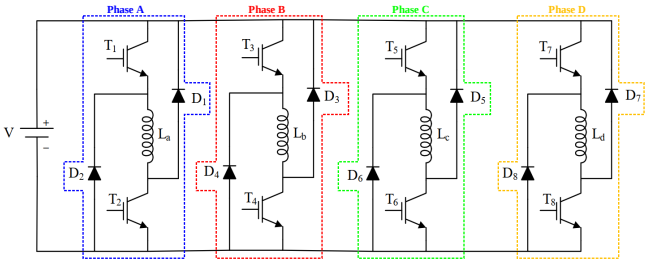

Fig. 2. The structure of 4-phase asymmetric bridges–power converter used in SRM drive

2. Modeling of SRM Drive

noindent With neglecting the hysteresis effects and eddy currents, the relation of voltage per phase could be considered as follow:

$$V_S = R_s i_s + \frac{d\lambda_s(\phi_s, i_s)}{dt} \tag{1}$$

where, V_S is supplied voltage, R_s is the resistance of s-th phase, i_s indicates phase current of s-th phase, t is time, and λ_s shows the phase flux linkage of s-th phase that is a function of position (ϕ_s) and current, and could be expressed as follows:

$\lambda_s(\phi_s, i_s) = L_s(\phi_s, i_s)\, i_s$

where, L_s is the phase inductance of s-th phase. By replacing (2) in (1), the new equation of voltage could be as (2), which includes three terms of dropped voltage by resistance, dropped voltage by inductance, and back Electro–Magnetic Force (EMF).

$$\begin{aligned} V_S =& R_s i_s + \frac{d}{dt}\{L_s(\phi_s, i_s)\, i_s\} = R_s i_s + L_s(\phi_s, i_s)\frac{di_s}{dt} \\ &+ \omega i_s \frac{d}{d\phi}\{L_s(\phi_s, i_s)\} \end{aligned} \tag{2}$$

The electromagnetic torque, T_e, could be calculated as follows:

$$T_e(\phi_s, i_s) = T_L + J\frac{d\omega}{dt} + B\omega \tag{3}$$

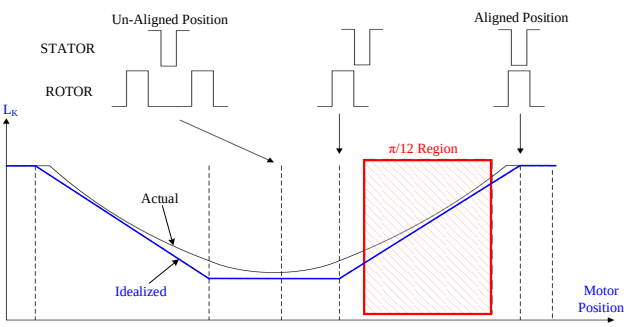

Fig. 3. The inductance of 4/8 poles, four phases SRM

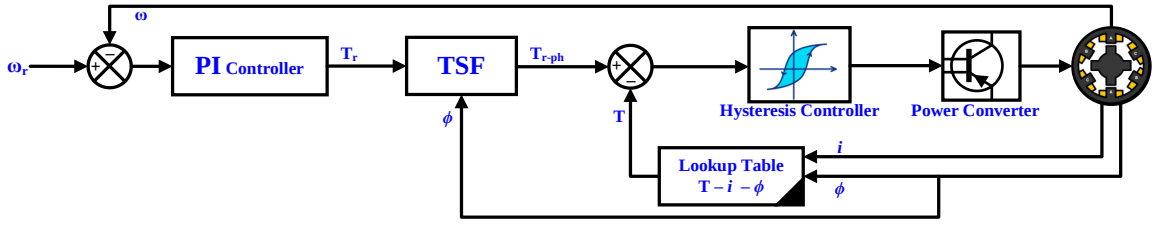

Fig. 4. The inductance of 4/8 poles, four phases SRM

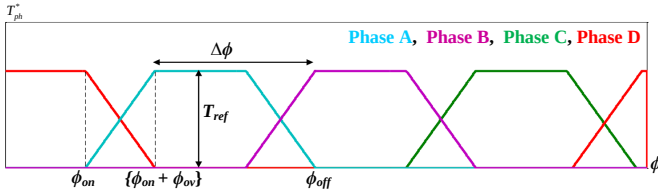

(a)

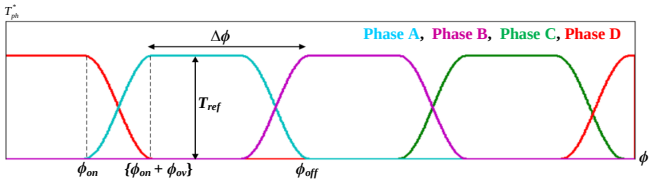

(b)

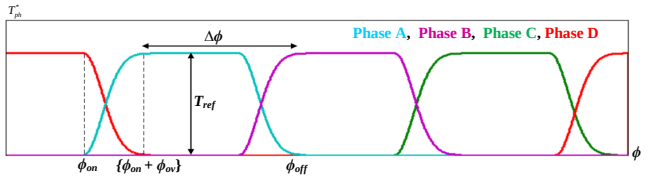

(c)

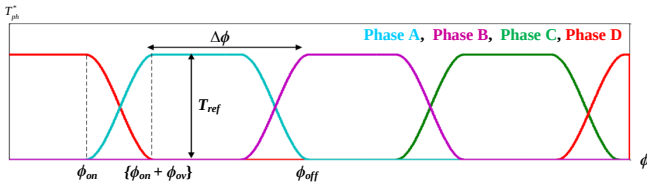

(d)

Fig. 5. The curve of TSFs, (a) LTSF, (b) STSF, (c) ETSF, (d) CTSF

where, T_L is load, inertia moment is introduced by J, ω is rotational speed, and B indicates the friction coefficient. Besides, the electromagnetic torque could be calculated as follows:

$$T_e(\phi_s, i_s) = \frac{i_s^2}{2}\frac{d}{d\phi_s}\{L_s(\phi_s, i_s)\} \tag{4}$$

Finally, the description of the relation between the electro–magnetic and the mechanical domains of the SRM could be as follows:

$$\frac{i_s^2}{2}\frac{d}{d\phi_s}\{L_s(\phi_s, i_s)\} - T_L = J\frac{d\omega}{dt} + B\omega \tag{5}$$

The behavior of an SRM could be described by (2) and (5). In these equations, ω and i_s are the state variables, and their multiplication shows the nonlinear behavior of SRM. Therefore, a development controller should linearize this behavior. The structure of the studied SRM is shown in Fig. 1.

Fig. 2 shows the structure of the used power converter as a supply source of the SRM. As seen in this structure, per phase per pole, there are two switches. When phase A should be turned on, the gate command is given to the switches T_1 and T_2, and the supply voltage is placed on both ends of the stator phase windings ($V_{ph} = V_{dc}$). Therefore, the current starts to increase, which is a function of stator windings inductance and the voltage of the power source. In this case, there will be a little power loss. When phase A has to be turned off, the switches T_1 and T_2 will be turned off ($V_{ph} = -V_{dc}$). However, due to the inductor current cannot being cut off suddenly, a huge voltage is generated at both ends that tend to maintain the current. To solve this problem, two diodes are installed in the circuit to remove the energy stored in the phase without damaging the switches. When the switches are turned off, these diodes form a path for the inductor current, which flows from negative to positive poles. In this way, the supply voltage is placed inversely on both ends of the considered phase and the power supply is charged. Obviously, if the supply voltage is higher, the both of increasing and decreasing rates will also be faster. The current equation could be formed as follows:

$$\frac{di_s}{dt} = \frac{1}{L_s(\phi_s, i_s)}\left(V_S - R_s i_s - i_s\omega\frac{dL_s(\phi_s, i_s)}{d\phi}\right) \tag{6}$$

According to Fig. 2, the power converters used in this paper are asymmetric bridges with two switches and two diodes in each phase. The main advantage of this converter is its control flexibility, which allows each phase to be controlled separately, especially in high-speed applications (like EVs) when commutation occurs between the adjacent phases. Besides, the main disadvantage may be the need for high-power components, which increases the cost and size.

3. Control Method Based on TSF

The output torque in the SRMs is obtained from the sum of the output torques in each phase, and each phase can produce the desired torque in a certain range. So, to distribute the torque generation task between all phases, it is necessary to identify the positions of each phase that can produce the highest torque at these positions. For example, consider a 4/6 poles, three phases SRM. In this SRM, the rotor pole-pitch is $\pi/2$. Therefore, each stator pole produces clockwise torque in half of the period ($\pi/4$) and counterclockwise torque in the other half. On the other hand, because the motor is three-phase, each phase must produce torque at $\pi/6$ in the same direction as the principal component, for completion $\pi/2$. Now, assuming a 4/8 poles, four phases SRM, the rotation period of the rotor is equal to $\pi/3$, and each pole in each period can produce $\pi/6$ of torque in the same direction as the principal component. Due to the number of phases being 4, each phase should produce the desired torque at $\pi/12$. Fig. 3 shows the inductance curves and areas for generating clockwise and counterclockwise torques for the last mentioned SRM [31]. In this figure, let's consider the $\pi/6$ region that could generate torque. In this region, an $\pi/12$ sub-region should be selected, which includes the best performance in producing torque. If the selected region is closed to the non-aligned position, due to the low value of $dL/d\phi$, at the beginning of each phase excitation, a large current needs to be injected to produce torque. Therefore, a high value of power in the commutation region will be lost. Also, if this region is closed

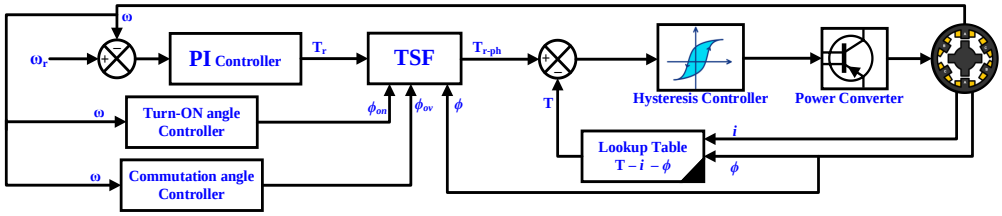

(a)

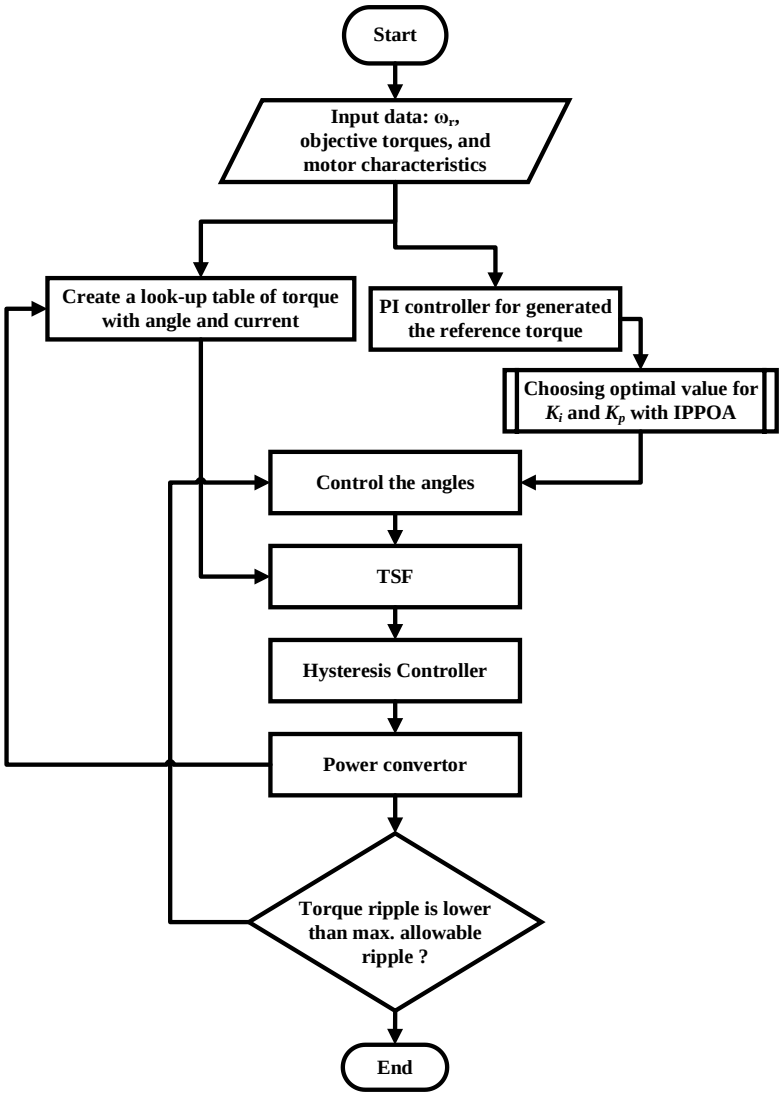

(b)

Fig. 6. The proposed control method for SRM: a) block diagram, b) flowchart

Table 1. The characteristic of the studied SRM

Parameter	Value	Parameter	Value
Number of phases (m)	3	Inertia (J)	0.05
Number of stator poles (N_s)	8	Maximum current	450
Number of rotor poles (N_r)	6	Maximum flux	0.486
Stator resistance per phase (R_s)	0.2	Source Voltage (V_S)	300
Non–aligned inductance	0.0067	Friction coefficient (B)	0.02
Saturated aligned inductance	0.0015	Aligned inductance	0.0236

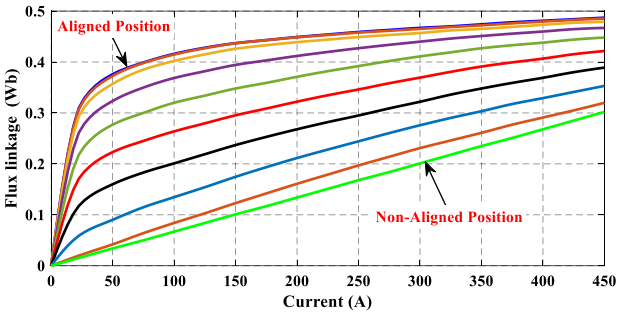

Fig. 7. The magnetic characteristic of the studied SRM

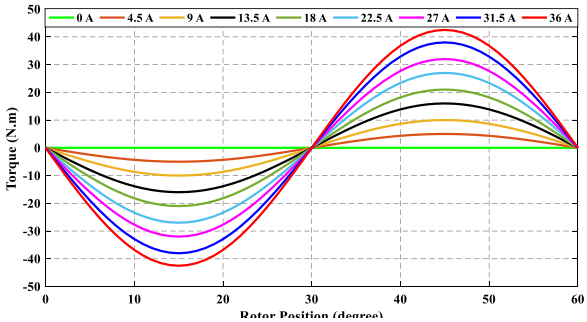

Fig. 8. The relations between torque–position–current of the studied SRM

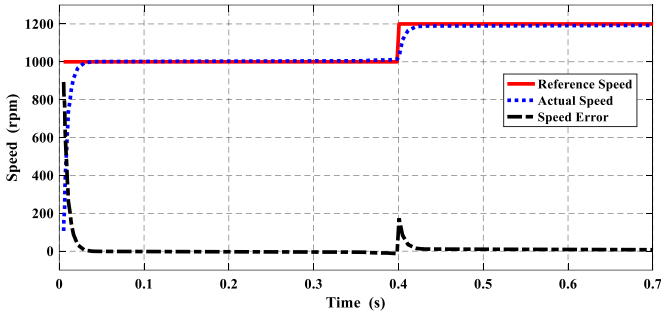

(a)

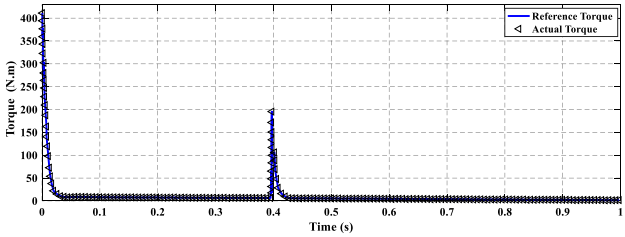

(b)

Fig. 9. The speeds and torque obtained in case 1, (a) The reference, obtained and error speeds, (b) The obtained torque

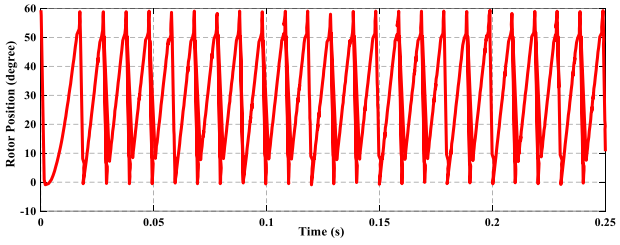

Fig. 10. The rotor position variations in case 1

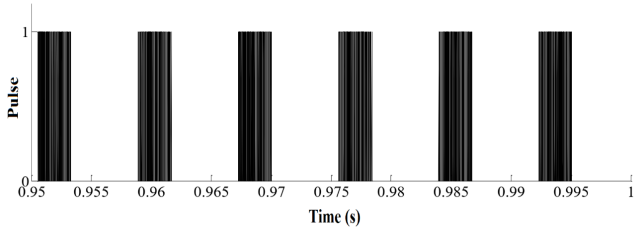

Fig. 11. The applied pulses to switches of phase A

Table 2. The summarized results for case 1

TSF type	T_{av} (N.m)	T_{max} (N.m)	T_{min} (N.m)	Torque Ripple (%)
LTSF	17.53	19.28	15.87	19.42
STST	17.53	19.77	15.58	23.89
ETSF	17.53	20.77	15.51	30.06
CTSF	17.53	19.61	15.58	22.96

to the aligned position, the value of dL/dϕ is low again. However, due to a large amount of inductance near the aligned position and the lack of rapid current discharge, it causes a delay in current reduction at commutation and produces negative torque. For this purpose, by omitting the saturation effect, the value dL/dϕ can be calculated between the aligned and non–aligned positions. Then, the π/12 sub-region with the highest dL/dϕ will be selected as the desired area. In the case of considering the saturation effect, since the inductance is a function of both rotor position and current, proportional currents should be proposed for different torques. Then, the areas of π/12 with the highest level will be selected. Due to the applied current to one phase cannot be changed with a high slope, it is not possible that the produced torque to be zero by one phase at a special moment and bring the output torque of the other phase to the desired value in a short moment. Therefore, for the moments of commutation, the amount of torque produced by each phase as well as its changing process should be determined. Therefore, the TSF has been introduced that the output torque of each phase changes based on specific mathematical functions. This method is a control process to produce a continuous uniform torque to reduce the torque ripple. Also, it uses some special sharing functions for generating the reference torques.

Fig. 4 illustrates a block diagram of the TSF control method for SRM with four phases. This method includes some main steps. First, a reference speed (ω_r) is determined and compared with the motor speed. Second, the resulting error is given to a PI control block to produce the reference signal of the torque. Third, this signal is decomposed into TSFs proportional to each of the phases, while the sum of the reference torques of all phases at any given moment is equal to the total reference torque. Fourth, the reference output torque is compared with the actual torque signals of each

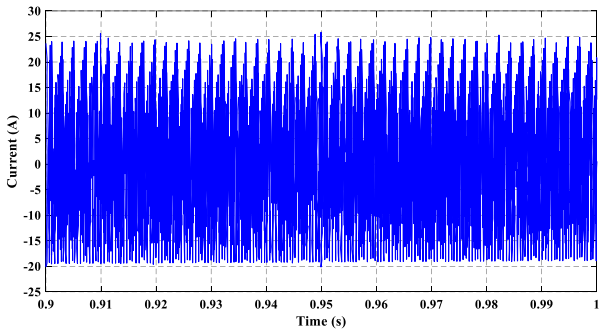

Fig. 12. The current variation of the DC source

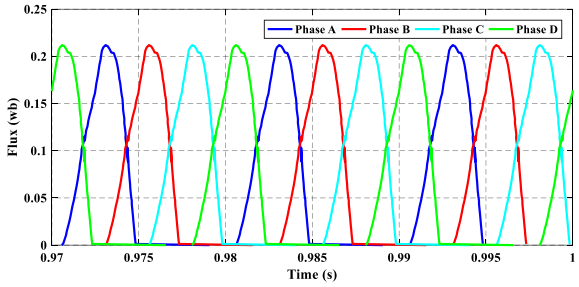

(a)

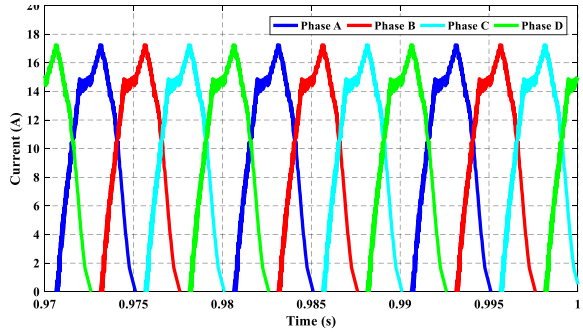

(b)

Fig. 13. The flux and current variation of all phases, (a) Flux, (b) Current

phase, and their errors are applied to the torque hysteresis control block. Fifth, the hysteresis block applies switching pulses to the electronic power converter for starting the motor [32]. Note that to generate the reference torques of each phase, the rotor position signal is also necessary, which is obtained from the position sensor data or estimating methods. In this paper, the second method is used.

3.1. The Linear TSF

The Linear TSF (LTSF) indicates that the torque produced by each phase in the commutation interval could be determined as a linear function based on the rotor position. The equations of LTSF are as follows:

$$T_{ph}^{*}=\begin{cases} T_{ref}\frac{\phi-\phi_{on}}{\phi_{ov}} & \phi_{on}\le\phi<\phi_{on}+\phi_{ov} \\ T_{ref} & \phi_{on}+\phi_{ov}\le\phi<\phi_{off}-\phi_{ov} \\ T_{ref}\frac{\phi_{off}-\phi}{\phi_{ov}} & \phi_{off}-\phi_{ov}\le\phi<\phi_{off} \end{cases} \quad (7)$$

where, ϕ_{on}, ϕ_{off}, and ϕ_{ov} are the turn-on, turn-off, and overlapping angles, respectively. Besides, T_{ref} is the total desired torque. The mentioned parameters are determined in the LTFS curve for four phases in Fig. 5(a).

3.2. The Sinusoidal TSF

In the Sinusoidal TSF (STSF), the output torque of each phase in the commutation interval is a sine function according to the position of the rotor, which is defined as with (8). Also, the curve of STSF for four phases is plotted in Fig. 5(b).

$$T_{ph}^{*}=\begin{cases} T_{ref}\sin^{2}\left(\frac{\pi}{2}\frac{\phi-\phi_{on}}{\phi_{ov}}\right) & \phi_{on}\le\phi<\phi_{on}+\phi_{ov} \\ T_{ref} & \phi_{on}+\phi_{ov}\le\phi<\phi_{off}-\phi_{ov} \\ T_{ref}\sin^{2}\left(\frac{\pi}{2}\frac{\phi_{off}-\phi}{\phi_{ov}}\right) & \phi_{off}-\phi_{ov}\le\phi<\phi_{off} \end{cases} \quad (8)$$

3.3. The Exponential TSF

The defined function of the Exponential TSF (ETSF) is as follows:

$$T_{ph}^{*}=\begin{cases} T_{ref}\left[1-\exp\left(-\frac{(\phi-\phi_{on})^{2}}{\phi_{ov}}\right)\right] & \phi_{on}\le\phi<\phi_{on}+\phi_{ov} \\ T_{ref} & \phi_{on}+\phi_{ov}\le\phi<\phi_{off}-\phi_{ov} \\ T_{ref}\exp\left(-\frac{(\phi_{off}-\phi_{ov}-\phi)^{2}}{\phi_{ov}}\right) & \phi_{off}-\phi_{ov}\le\phi<\phi_{off} \end{cases} \quad (9)$$

The curve of ETSF for four phases is shown in Fig. 5(c).

3.4. The Cubic TSF

The Cubic TSF (CTSF) is defined base on a cubic algebraic function. As seen in (10), the desired function is non-linear. The curve of CTSF for four phases is shown in Fig. 5(d).

$$T_{ph}^{*}=\begin{cases} T_{ref}\left[3\left(\frac{\phi-\phi_{on}}{\phi_{ov}}\right)^{2}-2\left(\frac{\phi-\phi_{on}}{\phi_{ov}}\right)^{3}\right] & \phi_{on}\le\phi<\phi_{on}+\phi_{ov} \\ T_{ref} & \phi_{on}+\phi_{ov}\le\phi<\phi_{off}-\phi_{ov} \\ T_{ref}\left[1-3\left(\frac{\phi-\phi_{off}+\phi_{ov}}{\phi_{ov}}\right)^{2}+2\left(\frac{\phi-\phi_{off}+\phi_{ov}}{\phi_{ov}}\right)^{3}\right] & \phi_{off}-\phi_{ov}\le\phi<\phi_{off} \end{cases} \quad (10)$$

Table 3. The summarized results for case 2

TSF type	T_{av} (N.m)	T_{max} (N.m)	T_{min} (N.m)	Torque Ripple (%)
LTSF	17.52	18.93	16.08	16.22
STST	17.52	19.52	15.94	20.42
ETSF	17.52	20.16	15.11	28.94
CTSF	17.52	19.46	16.07	19.31

3.5. The Optimization Criteria of TSFs

Although the TSF could reduce the torque ripple of SRM, the copper losses are dependent on the TSF type and its parameters. Therefore, selecting a robust TSF is essential. The selected TSF type also affects the speed range with acceptable torque ripple as well as the phase current peak. Because the values of ϕ_{on}, ϕ_{off}, and ϕ_{ov} are interdependent, the number of TSF parameters can be reduced to only two parameters. The relationship between TSF parameters is as follows:

$$\phi_{off}=\phi_{on}+\phi_{ov}+\Delta\phi \quad (11)$$

where, $\Delta\phi$ is the stroke angle that is the displacement angle between consecutive phases, and is defined as follows:

$$\Delta\phi=\frac{2\pi}{mN_{r}} \quad (12)$$

where, m is the number of phases, and N_r is the number of rotor poles. Besides, a new parameter as the central angle is defined that two consecutive phases have the same torque (equal to half of T_{ph}^{*}) at this point. This angle, based on Fig. 4, could be defined as follow:

$$\phi_{C}=\phi_{on}+\phi_{ov}/2=\phi_{off}-\Delta\phi-\phi_{ov}/2 \quad (13)$$

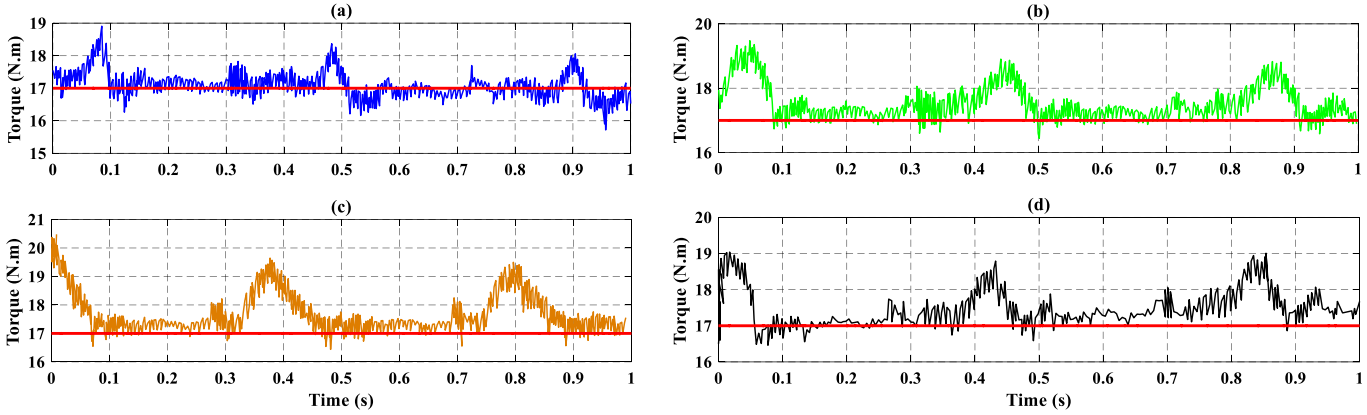

Fig. 14. The results of torque for phase A in case 1, (a) LTSF, (b) STSF, (c) ETSF, (d) CTSF

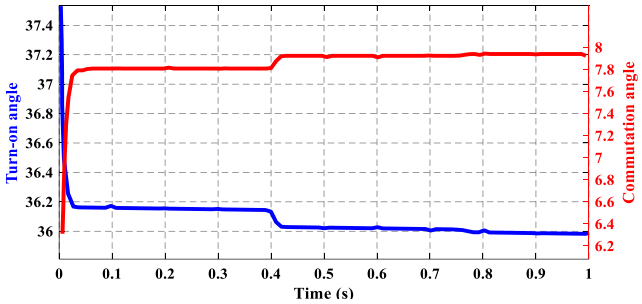

Fig. 15. The variation of angles in case 2

In the cases of minimum turn-on angle and maximum turn-off angle, the maximum overlapping angle could be obtained as $\phi_{ov}^{MAX} = \tau/4$, which τ is the pole pitch.

3.6. The Controlling of Angles

In some works, the turn-on angle is pulled back until the torque error reaches the desired value. The aim of this paper is based on the reduction of turn-on angle and combination with the commutation angle control method in order to reduce the torque ripple at high speeds. The variations of turn-on angle and speed are stored in a lookup table. Then, the turn-on angle, in proportion to the speed, tends to the aligned angle. In this method, the values of turn-on angle are optimized by optimization algorithms.

If speed increases, the turn-on and turn-off angles decrease, which leads to an increment of the current peak at the beginning of the phase conduction. So, to prevent a large increase in current and prevent torque drop, the commutation range will be raised by increasing the commutation angle. Therefore, the optimal values of the commutation angle are always within the expected range and are increased in proportion to the increment of speed that is stored in a lookup table. The final sketch of the proposed method for controlling the SRM used in EVs is shown in Fig. 6.

4. The Simulation Results

The characteristic of the studied SRM is tabulated in Table 1. Also, the magnetic characteristic of this SRM is shown in Fig. 7, in which some parameters like aligned, non-aligned, and saturated aligned inductances, as well as the maximum allowable motor current, could be extracted. The torque–position–current curve is another important feature of each SRM, which is shown in Fig. 8. As seen in this figure, in ϕ = 0, the stator and rotor poles are in the aligned position, and in ϕ = π/6 are in the non-aligned position. The flux of each phase could be calculated as follow:

$$\lambda_s = \int [V_S - R_s I_s]\, dt \tag{14}$$

The torque ripple could be calculated as follow:

$$T_{ripple}(\%) = \frac{T_{\max} - T_{\min}}{T_{avg}} \times 100 \tag{15}$$

The proposed control method based on TSF is evaluated in two different modes: 1) the introduced TSFs in the previous section are used without controlling turn-on, turn-off, and commutation angles; 2) the same TSFs are employed and turn-on and commutation angles are controlled. The results of two cases are compared at high speeds.

4.1. The Results of Case 1

In this case, based on Fig. 4, the torque is determined from the feedback of the PI controller. Also, the load toque is 15 N.m. The curve of reference and obtain speeds, and the error between these speeds are shown in Fig. 13(a). Moreover, the obtained torque from this error is presented in Fig. 13(b).
The variation of the rotor position is shown in Fig. 10. As seen in this figure, the period of rotor position reduces with increasing the rotor speed and is fixed in steady-state. The applied pulses to switches of phase A are based on Fig. 11. Also, the current variations of the DC source are presented in Fig. 12. The results of voltages and currents of all phases are shown in Fig. 13.
During the simulation, to limit the peak current in the phase turned-on moment, the turn-on angle for phase A is adjusted to 5.37° according to the positive and negative torque generation intervals. Also, the optimal turned-off angle is slightly less than the phase-aligned angle (59°) to prevent the production of negative torque, which leads to a high torque ripple. The commutation angle of all phases is also set at a constant value of 5.6°. In this case, all three angles, i.e. turn-on, turn-off, and commutation, have a constant value for each phase at different speeds. The reference and actual torques for phase A with various TSFs are shown in Fig. 14. The summarized results from these figures are listed in Table 2. According to Table 2, it can be seen that the torque ripple, in this case, is slightly higher. Therefore, using this idea that by increasing the speed, bringing the turn-on angle closer to the non-aligned angle, and combining it with increasing the commutation angle, in the next step, the torque ripple could be improved.

4.2. The Results of Case 2

The simulation method, in this case, is based on the block diagram in Fig. 6 with the same reference speed and a load torque of case 1. The turn-on angle variations, which are estimated at different speeds using the lookup table, are shown in Fig. 15. As seen in this figure, the turn-on angle tends to be the non-aligned angle as the velocity increases to decrease the torque ripple at

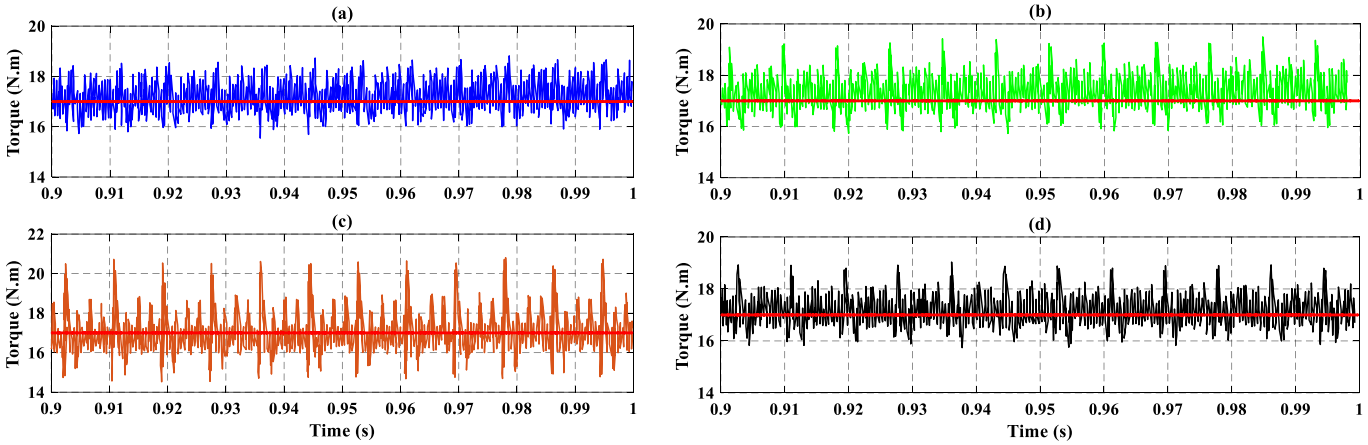

Fig. 16. TThe results of torque for phase A in case 2, (a) LTSF, (b) STSF, (c) ETSF, (d) CTSF

high speeds. Besides, the variations of the commutation angle are shown in Fig. 1. It should be noted that in this case, the turn-off angle is set to a constant value (44° for phase A). The turn-off angle of the other phases is set with a favorable shift relative to phase A. The results of phase A for various TSFs are plotted in Fig. 16, and the summarized results obtained from Fig. 16 are shown in Table 3.

Based on Table 3, it can result that the torque ripple has improved compared to case 1, due to the favorable changes in turn-on and commutation angles in proportion to the speed increase. It causes avoiding two states: entering the current into the negative zone of the torque and generating the peak current in the starting the phase conduction.

As shown in Fig. 16, the input of the power converter is the torque signals, to generate the requested voltage. Therefore, the consumption power of the switches is related to the torque values. Table 3 shows the torque ripples with various methods that indicate the power loss of switches. So, by applying the proposed method, the power loss will be reduced.

4.3. Applying the proposed method in a case study: electrical vehicle

As mentioned before, an EV uses the negative and positive torques, continuously. Therefore, in this section, these movements are simulated and the proposed method is applied. The PI controller has two main coefficients as K_p and K_i, which are optimized using the Improved Prey Predator Optimization Algorithm (IPPOA) [33] under each movement, which leads to better tracking of the reference velocity curve. In this case, the variations of reference and actual speeds are presented in Fig. 17(a), and the needed torque is plotted in Fig. 17(b). The simulation results for turn-on and commutation angles are shown in Fig. 18. The reference torque waveform and the actual torque for phase A for various TSFs are shown in Fig. 19. The obtained values for torque ripple show that it is again improved compared to case 2, due to the optimal selection of PI coefficients. This is the most common control of an SRM based on TSFs with a speed controller that turn-on and commutation angles are applied based on a lookup table. As the turn-on angle reduces to the non-aligned angle, the copper losses are also reduced more. Therefore, the drive efficiency will be enhanced. In this paper, the turn–on angle is reduced to 36°, while in other methods it reached 33°.

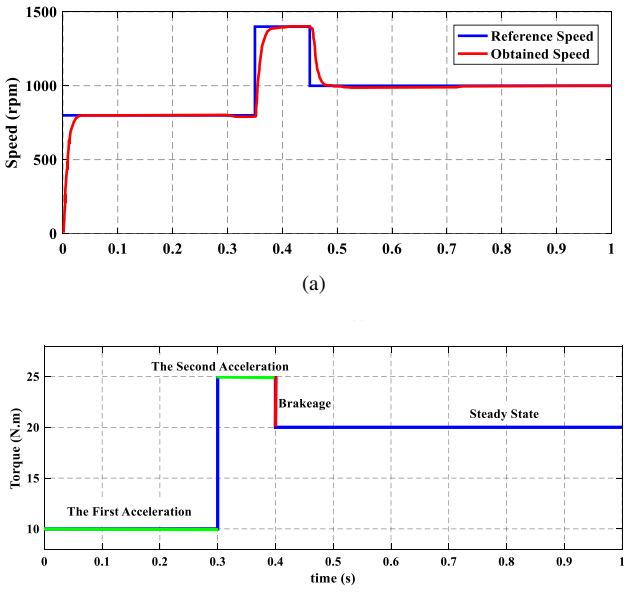

Fig. 17. The requested features of an SRM employed in EV, (a) speed, (b) torque

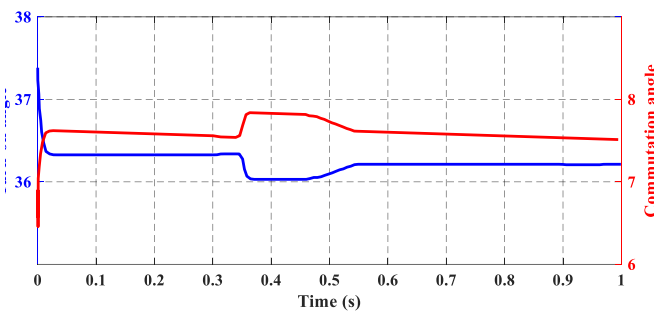

Fig. 18. The variation of angles of an SRM employed in EV, (a) turn-on angle, (b) commutation angleF

5. CONCLUSIONS

In this paper, a novel method is proposed and evaluated for the aim of MTRPT of an SRM applied in EV, based on various TSFs. The simulations are performed in various cases, and the results show better performance of the controller:

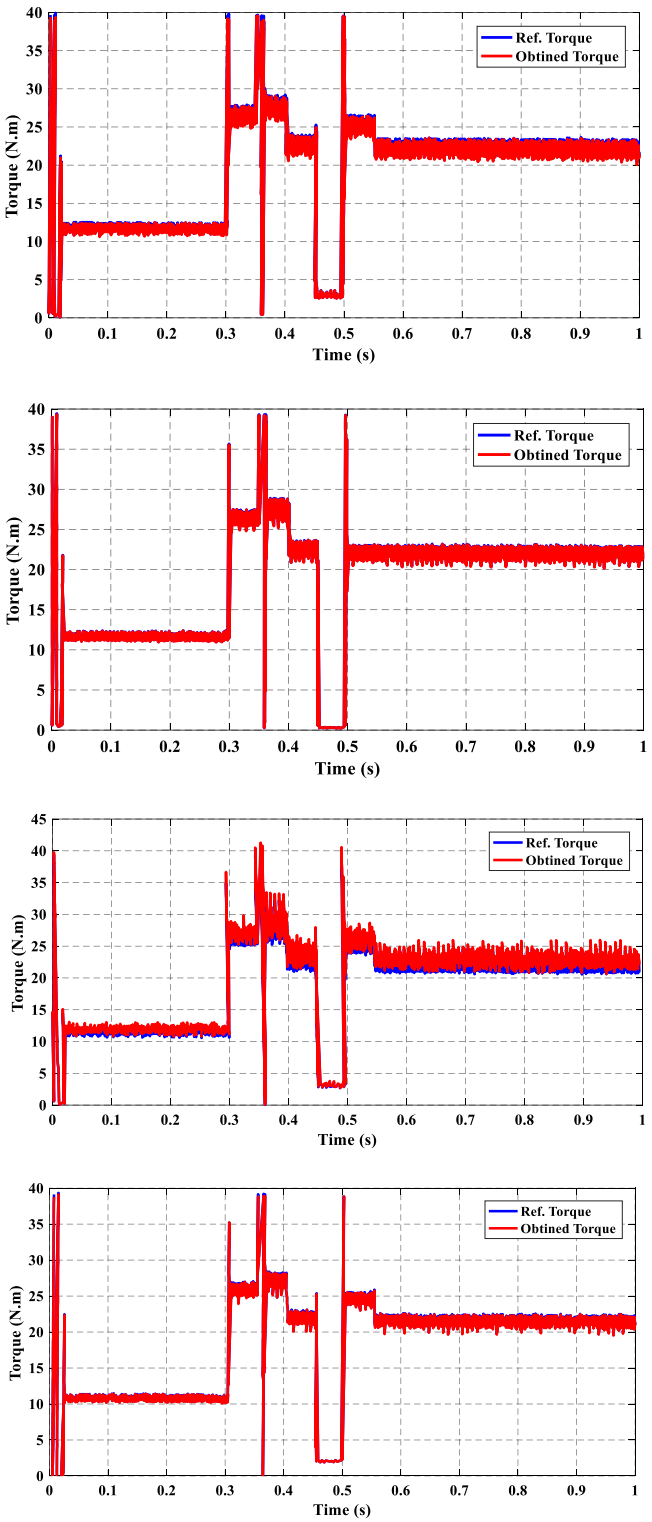

Fig. 19. The results of torque for phase A of the SRM employed in EV, (a) LTSF, (b) STSF, (c) ETSF, (d) CTSF

- In the first case, all angles are assumed as fixed, and the average torque ripple is obtained at about 24%. In this case, the LTSF was better than other TSFs.
- In the second case, the speed was higher than in case 1, and the angle database is considered with a lookup table to decrease the computational volume. To avoid large fluctuations in current, at the beginning and end of the conduction range, the phase shift values are optimally selected. In this case, the turn-on and commutation angles are controlled and the mean value of the torque ripple was about 20%, which is declined in comparison with case 1.
- Finally, the proposed control method is applied in an EV, which needs to continuously brake and accelerate. First, it accelerated, and then braked to assess the performance of the method and its response speed. The results are acceptable and the angles variated as fast as in case 2.
- The coefficients of the PID are optimized with IPPOA that could response very faster than other methods.

It should be noted that if this control method is performed for SRM with more poles, much less torque ripple will be obtained.

REFERENCES

[1] I. Boldea, ,L.N. Tutelea, ,L. Parsa, and D. Dorrell, "2014. Automotive electric propulsion systems with reduced or no permanent magnets: An overview," *IEEE Trans. Indust. Electron.*, 61(10), pp.5696-5711.

[2] E. Bostanci, ,M. Moallem, A. Parsapour, and B. Fahimi, "Opportunities and challenges of switched reluctance motor drives for electric propulsion: A comparative study," *IEEE Trans. Transp. Electrif.* ,3(1), pp.58-75, 2017.

[3] M.V. de Paula, and T.A. dos Santos Barros, "A New Flux Linkage Estimation with Drift Cancellation Technique for Switched Reluctance Machines," *Electronics*, 9(3), p.405, 2020.

[4] H. Li, ,B. Bilgin, and A. Emadi, "An improved torque sharing function for torque ripple reduction in switched reluctance machines, *IEEE Trans. Power Electron.*, 34(2), pp.1635-1644, 2018.

[5] M. Hamouda, ,A. Abdel Menaem, ,H. Rezk, ,M.N. Ibrahim, and L. Számel, "Comparative evaluation for an improved direct instantaneous torque control strategy of switched reluctance motor drives for electric vehicles," *Mathematics*, 9(4), p.302, 2021.

[6] G Mariappan, . and K. Lakshmanan, "An enhanced control method for torque ripple minimization of switched reluctance motor using hybrid technique," *J. Intell. Fuzzy Syst.* , (Preprint), pp.1-24, 2022.

[7] A.K. Rana, and A.R. Teja, "A mathematical torque ripple minimization technique based on a nonlinear modulating factor for switched reluctance motor drives," *IEEE Trans. Indust. Electron.*, 69(2), pp.1356-1366, 2021.

[8] H. Li, ,B. Bilgin, and A. Emadi, "An improved torque sharing function for torque ripple reduction in switched reluctance machines," *IEEE Trans. Power Electron.*, 34(2), pp.1635-1644, 2018.

[9] H. Cai, H. Wang, M. Li, S. Shen, Feng, Y. and J. Zheng, "Torque ripple reduction for switched reluctance motor with optimized PWM control strategy," *Energies*, 11(11), p.3215, 2018.

[10] S. Song, R. Hei, R. Ma, and W. Liu, . Model Predictive Control of Switched Reluctance Starter/Generator With Torque Sharing and Compensation," *IEEE Trans. Transp. Electrif.*, 6(4), pp.1519-1527, 2020.

[11] M.V. de Paula, dos Santos T.A. Barros, H.S. Moreira, Catata, E.H., Villalva, M.G. and E. Ruppert Filho, "A dahlin cruise control design method for switched reluctance motors with minimum torque ripple point tracking applied in electric vehicles," *IEEE Trans. Transp. Electrif.*, 2020

[12] S.S. Ahmad, and G. Narayanan, "Linearized modeling of switched reluctance motor for closed-loop current control. *IEEE Trans. Indust. Appli.*, 52(4), pp.3146-3158, 2016.

[13] Q. Ma, ,E.R. Ayman, and J.S. Lai, "September. Small-signal modeling and speed controller design for switched reluctance motor drives," *IEEE Energy Conversion Cong. Exposi. (ECCE)* (pp. 4497-4504). IEEE, 2018.

[14] W. Peng, ,J. Pelletier, ,Y. Mollet, and J. Gyselinck, September. Torque Sharing Function and Firing Angle Control of Switched Reluctance Machines-Hysteresis Current Control Versus PWM," *Int. Conf. Elec. Machines (ICEM*) (pp. 1717-1723). IEEE, 2018.

[15] S. Mehta, I. Husain, and P. Pramod, September. Predictive current control of mutually coupled switched reluctance motors using net flux method," *IEEE Energy Conversion Cong. Expos. (ECCE)* (pp. 4918-4922). IEEE, 2019.

[16] S. Mehta, ,P. Pramod, and I. Husain, June. Analysis of dynamic current control techniques for switched reluctance motor drives for high performance applications. In 2019 IEEE Transportation Electrification Conference and Expo (ITEC) (pp. 1-7). IEEE, 2019.

[17] X. Zhang, ,Q. Yang, ,M. Ma, ,Z. Lin, and S. Yang, . A switched reluctance motor torque ripple reduction strategy with deadbeat current control and active thermal management," *IEEE Veh. Technol. Mag.* 69(1), pp.317-327, 2019.

[18] S. Walz, R. Lazar, Buticchi, G. and M. Liserre, "Dahlin-based fast and robust current control of a PMSM in case of low carrier ratio," *IEEE Access*, 7, pp.102199-102208, 2019.

[19] S. Mehta, Kabir, M.A., Pramod, P. and Husain, I. Segmented Rotor Mutually Coupled Switched Reluctance Machine for Low Torque Ripple Applications," *IEEE Trans. Indus. Appli.*, 2021.

[20] M. Hamouda, A.A. Menaem, H. Rezk, M.N. Ibrahim, and Számel, L., "An improved indirect instantaneous torque control strategy of switched reluctance motor drives for light electric vehicles," Energy Reports, 6, pp.709-71, 2020.

[21] Z. Xia, B. Bilgin, S. Nalakath, and A. Emadi, "A New Torque Sharing Function Method For Switched Reluctance Machines With Lower Current Tracking Error," *IEEE Trans. Indust. Electron.*, 2020.

[22] B. Bilgin, B. Howey, A.D. Callegaro, J. Liang, M. Kordic, J. Taylor, and A. Emadi, "Making the case for switched reluctance motors for propulsion applications," *IEEE Veh. Technol. Mag.* 69(7), pp.7172-7186, 2020.

[23] C. Li, C. Zhang, J. Liu, and D. Bian, "A High-Performance Indirect Torque Control Strategy for Switched Reluctance Motor Drives. *Math. Probl. Eng.*, 2021.

[24] A. Gholipour, M. Ghanbari, E. Alibeiki, and M. Jannati, "Sensorless FOC Strategy for Current Sensor Faults in Three-Phase Induction Motor Drives," *J. Oper. Autom. Power Eng., 2021.*

[25] H. Dahmardeh, M. Ghanbari, and S.M. Rakhtala, "A novel combined DTC method and SFOC system for three-phase induction machine drives with PWM switching method. J. Oper. Automa. Power Eng., 11(1), pp. 1-10, 2023.

[26] M. Nikpayam, M. Ghanbari, A. Esmaeli, and M. Jannati, "Vector Control Methods for Star-Connected Three-Phase Induction Motor Drives Under the Open-Phase Failure. J. Oper. Autom. Power Eng., 10(2), pp.155-164, 2022.

[27] M.V. de Paula, E.O.H. Catata, E. Ruppert Filho, dos Santos Barros, T.A. and Williamson, S., November. Direct Instantaneous Torque Control of Switched Reluctance Machines for Low Torque Ripple Regenerative Braking," *Brazilian Power Electro. Conf. (COBEP)* (pp. 1-5). IEEE, 2021.

[28] M.V. De Paula, and T.A. dos Santos Barros, "A sliding mode DITC cruise control for SRM with steepest descent minimum torque ripple point tracking," *IEEE Trans. Indust. Electron.*, 69(1), pp.151-159, 2021.

[29] P. Ren,, J. Zhu, Jing, Z., Z. Guo, and A. Xu, "Minimization of torque ripple in switched reluctance motor based on MPC and TSF," *IEEE Trans. Elect. Electron. Eng.*, 16(11), pp.1535-1543, 2021.

[30] Z. Yu, C. Gan, K. Ni, R. Qu, and W. Kong, "Dual Three-Phase Flux-Modulated Switched Reluctance Motor Drive With Maximum Torque per Ampere Strategy," *IEEE Trans. Indust. Appli.*, 57(2), pp.5806-5817, 2021.

[31] V.P. Vujičić, "Minimization of torque ripple and copper losses in switched reluctance drive," *IEEE trans. power electron.*, 27(1), pp.388-399, 2011.

[32] J. Guo, X. Ma, and A. Ahmadpour, "Electrical–mechanical evaluation of the multi–cascaded induction motors under different conditions," *Energy*, 229, p.120664, 2021.

[33] A. Dejamkhooy, and A. Ahmadpour, "Optimal UC and economic dispatching with various small energy resources in the micro-grid using IPPOA and IMILP," *Energy Reports*, 7, pp.7572-7590, 2021.